Electron Scattering, Sendai, Japan 1972 (unpublished).

[24] K. Lips and M. T. McEllistrem, Phys. Rev. C 1, 1009 (1970).

[25] A. Bohr and B. Mottleson, *Nuclear Structure* (Benjamin, New York, 1969), vol. 1.

[26] R. A. Eisenstein, D. W. Madsen, H. Theissen, L. S. Cardman, and C. K. Bockelman, Phys. Rev. 188, 1815 (1969).

PHYSICAL REVIEW C VOLUME 7, NUMBER 3 MARCH 1973

Neutron Asymmetries and Energy Spectra from Muon Capture in Si, S, and Ca[†]

R. M. Sundelin[*] and R. M. Edelstein
Carnegie-Mellon University, Pittsburgh, Pennsylvania 15213

(Received 5 July 1972)

The energy dependence of the neutron asymmetry parameter for nuclear capture of muons has been measured in Si, S, and Ca for neutron energies of 4–53 MeV. Contrary to most recent experiments, the asymmetry parameter is strongly positive over much of the energy range, with values as much as 9 standard deviations from zero. Because of the unusual nature of these results the experiment was performed twice and with excellent agreement between the two sets of data. The integrated asymmetry parameter for $E_n > 15.6$ MeV is +0.316 ± 0.023 for Si and +0.290 ± 0.034 for Ca, values which are in direct conflict with the "standard" $V-A$ theory. Recent theoretical calculations by Bogan and by Piketty and Procureur obtain positive asymmetries, though not yet in good quantitative agreement with these data. The neutron energy spectra from the three targets are all quite similar. They are consistent with a simple exponential falloff in E_n with a decay constant of 7 MeV. The theoretical calculations cited above are in good agreement with higher-energy regions of the spectra.

I. INTRODUCTION

Since the first days following the discovery of parity violation in the weak interaction,[1] there has been a continuing interest in studying this phenomenon in the process of nuclear capture of muons. For reasons of practicality and difficulty, much of the theoretical work and all of the experiments have concerned themselves, in particular, with the asymmetry in the angular distribution of neutrons following muon capture.

The "standard" $V-A$ theory[2] for muon capture involves six real coupling constants, if second class currents are allowed, so that without *a priori* knowledge of them ⩾6 independent combinations must be determined from experiment in order to establish the validity of the theory. At the present time, for the most part, experiments are compatible with the "standard" theory, but they by no means form an overconstraining set from which to derive the coupling constants. Since most measurements of capture rates involve a statistical mixture of Fermi and Gamow-Teller couplings[3] they do not really measure independent combinations of constants (in addition to the difficulties of imprecise nuclear models). Thus, aside from demonstrating parity violation, the neutron asymmetry measurement is important, in principle, for the understanding of muon capture, since it measures an independent combination of constants. To lowest order in nucleon momentum, and neglecting differences in form factors, the capture rate for a statistical mixture of Fermi and Gamow-Teller interactions varies approximately as

$$G_V^2+3G_A^2+G_P^2-2G_PG_A,$$

where G_V, G_A, and G_P are the phenomenological vector, axial vector, and induced pseudoscalar coupling constants; whereas, the neutron asymmetry parameter is characterized by[2]

$$\alpha=\frac{G_V^2-G_A^2+G_P^2-2G_PG_A}{G_V^2+3G_A^2+G_P^2-2G_PG_A}$$

which yields the expected value $\alpha \approx -0.4$.

In reality, the neutron asymmetry parameter is not a sensitive test of weak-interaction theory, because of the uncertainty involved in the nuclear models, for any and all complex nuclei, as well as the final-state interactions of the neutrons produced in the process.[2, 4] It is expected that this rescattering reduces the observed asymmetry, but also that higher-energy neutrons will be less affected. It was further realized[5] that there may be local fluctuations in the neutron energy dependence of the asymmetry due to nonstatistical muon capture, as for example in the case of pure Fermi capture, which would give rise to a large positive asymmetry. Klein, Neal, and Wolfenstein[6] have shown that additional terms in the Hamiltonian, sensitive to the nucleon momentum, play an important role in the asymmetry parameter. Using a Fermi-gas nuclear model they have found a considerable decrease in the magnitude of the asymmetry when these terms are included. As Bogan has shown[7] with the same Hamiltonian, but with a shell model for the nucleus, the details of the energy dependence of the asymmetry are dependent on nuclear models, although his model still produces small asymmetries. Piketty and Procureur[8] have gone one step further and demonstrated that if second-order relativistic corrections to the Hamiltonian are included, the theory can be brought into rough agreement with the data of this experiment, although the asymmetry still tends to lie lower than the data.

These models will be discussed somewhat further in Secs. III and IV, but the conclusion to be reached is that neutron asymmetry experiments are not likely to lead to greater understanding of the fundamental weak interaction, because of complex questions of nuclear physics. On the contrary it is to be hoped that this type of experiment can be used as a tool for studying nuclear models, assuming the structure of the weak interaction to be known.

The history of the experiments in this field is also quite varied in large part because of the great difficulty in obtaining precise results. Most of the more recent experiments have quoted large negative asymmetries, so large in one case[9] as to require the introduction of unusual values of the coupling constants including possibly second-class currents to explain the result. In the series of experiments described in the present paper, which was performed at the Carnegie-Mellon University synchrocyclotron, the energy dependence of the neutron asymmetry parameter was studied in Si, S, and Ca from 4–53 MeV. They were begun with the hope of providing very precise, conclusive results. It was to our amazement that contrary to establishing the "final accurate negative values" of the asymmetries, our first experiment[10] yielded substantial *positive* asymmetries, particularly at larger neutron energies. Because of the unusual nature of the first result the experiment has been repeated with great emphasis being placed on checks of the data and on taking care to minimize systematic errors, while at the same time accumulating large numbers of events, more than the combination of all previous world data. The results of the two runs are in excellent agreement.

The data from these runs have also been used to measure the energy spectrum of the emitted neutrons as was first reported by Sundelin *et al.*[11] The same nuclear models used to fit the asymmetry data must also fit these spectra. However, the latter are a less sensitive test of the models than are the former. A detailed discussion of the spectra is given in Sec. IV.

II. EXPERIMENT

A. General Description

The experiment described in this paper consisted of three separate runs. In run I, the asymmetry in the angular distribution of neutrons emitted following capture of a polarized muon by a target nucleus was measured directly as a function of the neutron energy. The neutron energy was measured by time of flight, the start signal being provided by a nuclear deexcitation γ ray, and the stop signal being provided by the neutron whose energy was to be determined. This measurement, unsuccessful due to problems with rate and background, is discussed in Appendix A.

In runs II and III, the neutron asymmetry was measured as a function of the pulse height produced in a scintillation counter by charged-particle recoils from the neutron. Polarized negative muons were stopped in a target located in a uniform magnetic field. The muons were captured into an atomic orbit by a target nucleus, and their spins precessed due to the magnetic field until they decayed or were captured by the nucleus. A large-volume scintillation counter was placed at right angles to the muon beam line, and was used to detect electrons from muon decay and neutrons and γ rays emitted following muon capture by the nucleus. Electrons were distinguished from neutrons and γ rays by thin coincidence counters located between the target and the large-volume counter, and neutrons were distinguished from γ rays by pulse-shape discrimination. Two-dimensional analysis of each event was performed. The time between the stopping of the muon and the detection of a particle in the large-volume counter was measured by a 100-MHz digital timing system, and the pulse height in the large volume counter was measured by an eight-channel pulse-height analyzer. The neutron energy spectrum was determined by unfolding the pulse-height spectrum, using known cross sections for various interactions in the scintillator. The asymmetry was determined from the amplitude modulation of the digital timing spectrum caused by the precession of the muon in the magnetic field. Run III[12] differed from run II[10, 11] in that a cleaner and more intense muon beam was used, both directions of the precession field were used, an internal beam stretcher producing less time structure was used, and a number of improvements in the electronics were made. The description which follows applies to run III. Where an important difference from run II existed, the difference is described.

B. Physical Apparatus

1. Beam

The arrangement of the physical apparatus is shown in Fig. 1. The negative muon beam from the Carnegie-Mellon University 450-MeV synchrocyclotron passed through a muon channel of coaxial geometry with a direct current of 11 500 A. The magnetic field produced by the current in the center conductor, which had a diameter of 1.7 cm, caused the negative particles to accelerate toward it and to follow helical paths around it. These helical paths prevented the loss of some of the muons which entered the channel at angles to its axis, and also increased the retention of muons resulting from the decay of pions in flight in the channel.

The muon channel was 16.5 m long, with the last 2.7 m passing through a 90° bending magnet. A pair of quadrupoles at the end of the muon channel focused the muons on the target.

The muon channel used in run II was similar, but was only 9 m long and ended before the bending magnet, which provided only a 30° bend. The channel used in run III provided a more intense beam, permitted better shielding and more pion decays by virtue of its length, and provided better isolation from the neutral beam because of the larger bending angle. In both runs, the target was located at the center of a C magnet which provided the precession field.

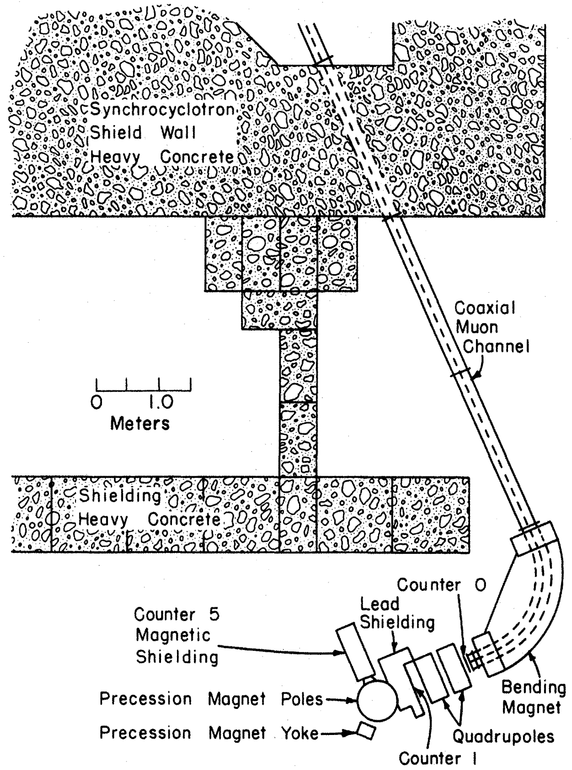

FIG. 1. Physical apparatus, large scale.

In run III, beam spill stretching was accomplished by using a carbon filament target in the beam midplane, and a carbon block target below the midplane. Vertical oscillations were induced by scattering in the carbon filaments, causing the beam to strike the carbon block. One proton bunch could be parked at the radius of the carbon filaments while another was being accelerated. Duty factors of 50% were achieved, with less than 5% residual 20.4-MHz structure in the beam.

In run II, a stochastic electrostatic cee was used to stretch the beam spill. This method of stretching retained the 20.4-MHz structure, and induced some structure around 100 kHz. The duty factor was 50%.

2. Counters

The arrangement of the counters is shown in Figs. 1 and 2. Counter 5 comprised a 19 cm-diameter by 12.7-cm-thick volume of NE-213 liquid scintillator viewed by a 58AVP photomultiplier. The front of the scintillant was 15.4 cm from the center of the target. This counter is described in detail in Appendix B. Counter Č was an acrylic Čerenkov counter. The remaining counters were ordinary plastic scintillation counters.

Counters 0 and Č were not used in run II.

3. Shielding

The shielding used in the vicinity of the target was primarily lead. Lead was chosen because muons in lead have a shorter lifetime than in any other readily available material. The short lifetime facilitates the analytical removal of background caused by muon stops in the shielding. In places where a muon stopping in the wrapping of a counter could be identified as a muon stopping in the target, the counter wrapping was made of 7 or 25 μm tantalum. Tantalum was used because of its strength and because muons have essentially the same lifetimes in lead and in tantalum, which similarity permitted the use of a single lifetime value in the high-Z background analysis.

4. Targets

The targets used in run II were silicon, sulfur, and calcium, and those used in run III were silicon and calcium. All targets were chemically pure. The effective target thickness in the direction of the beam was 4.0 g/cm^2. This thickness was chosen as an optimum compromise between muon stopping rate and scattering of the emergent neutrons and electrons. All targets used had spin zero to minimize the depolarization of the muons when they were captured into atomic orbits and to avoid theoretical complications associated with hyperfine structure.

5. *Muon Precession*

The muon beam was forward polarized in the direction of motion of the beam. Muons stopping in the target were precessed about a vertical axis by the field of the C magnet.

The current for the C magnet was supplied by a transistorized, regulated current supply having a long-term stability better than one part per thousand. The uniformity of the magnetic field over the target volume was measured to be better than 1%.

C. Electronics

A simplified block diagram of the electronics is shown in Fig. 3. Pulses from the counters, after being limited,[13] entered the fast logic, which identified muon stops and counter 5 events. Pulses from the fast logic were processed by slow logic, used to impose suitable requirements on the time relationships of muon stops and electrons, neutrons, or γ rays. Pulses from the slow logic were processed by the two-dimensional analyzer. One dimension was the time between the detection of a muon stop and the detection of an electron or neutron, and was measured by a 100-MHz digital timing system. The second dimension was the pulse height observed in counter 5, and was measured by an eight-channel pulse-height analyzer, one of whose channels was assigned to the registration of decay electrons. Each event, after being processed by the digital timing system and the eight-channel analyzer, was stored in a Victoreen SCIPP 1600-channel analyzer. The digital timing frequency used was 100 MHz for calcium and sulfur, and 50 MHz for silicon.

The following description applies to run III. Refer to Refs. 10 and 11 for a description of the electronics used for runs I and II.

1. *Logic*

The fast and slow logic are shown in greater detail in Fig. 4 (See the figure caption for definitions of symbols in this drawing.) A brief discussion follows:

The coincidence-anticoincidence $1234\bar{6}\bar{9}\bar{\check{C}}$ identified a muon stopping in the target, where $\bar{\check{C}}$ rejected electrons in the beam. The coincidence 569 identified a muon decay electron, and neutrons and γ rays in counter 5 were signaled by $5\bar{0}\bar{1}\bar{6}\bar{9}$, where $\bar{0}$ and $\bar{1}$ rejected neutrals from pions stopping in or near the target. Neutron- and γ-induced pulses in counter 5 were distinguished by the pulse-shape discriminator (PSD) which is discussed in detail in Appendix B. Muons stopping in the downstream portion of counter 4 were virtually eliminated from the muon sample by the further re-

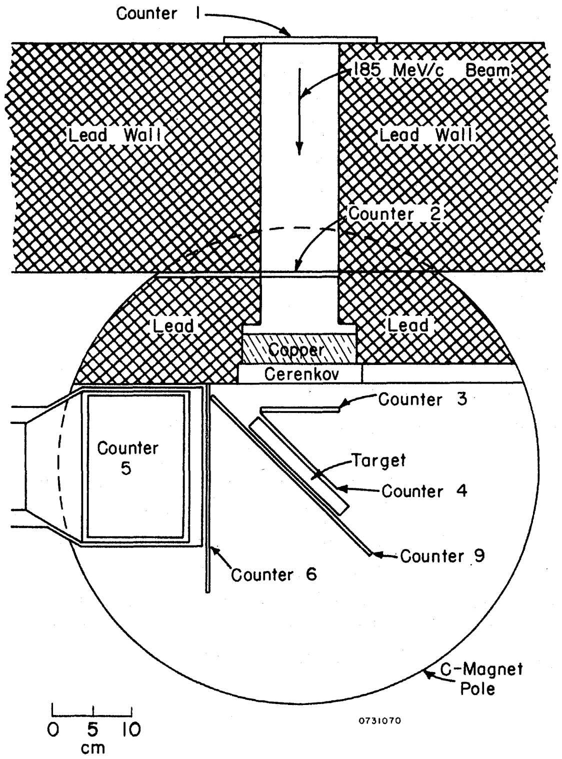

FIG. 2. Physical apparatus, small scale.

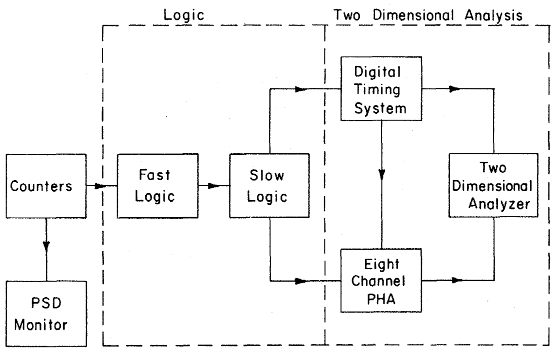

FIG. 3. Electronics block diagram.

quirements $3T$, $\overline{3H}$, and $\overline{4H}$ as discussed by Sundelin and Takahashi,[14] and the whole system was gated off during periods of high beam intensity. A stopping muon pulse served to start the digital timing circuitry, but only if: (a) there was no second muon within −30 and +10 μsec of the first, and (b) there was a valid stop pulse.

A stop pulse to the digital timing circuit was generated whenever there was a valid electron or neutral event in counter 5. In addition, dead-time circuitry provided that no counter 5 pulse occurred between −20 and +5.25 μsec of the stop pulse. The dead-time coverage was such that the accepted event rate went completely to zero as the average input event spacing became small compared to the minimum acceptable pair spacing. It also provided that no spurious time dependence was introduced into the time spectrum as sometimes happens in these measurements.

2. *Two-Dimensional Analyzer*

The two-dimensional analyzer system is shown in Fig. 5. As mentioned above timing information was stored in eight segments of the SCIPP analyzer. If an electron was signaled, the timing data were sent to the first segment; otherwise pulse height in counter 5 was analyzed in seven channels for routing the timing data to the other seven segments.

The timing data consisted of oscillator pulses (either 50 or 100 MHz) gated by the start-stop time difference into a Chronetics 100-MHz scaler. Note that the time gate also provided a dead time of 350 μsec so that a second start pulse during this time was ignored. Also, there were several stages of buffering between the oscillator and the 100-MHz scaler to insure a scaler response independent of the pulse train length. Finally, com-

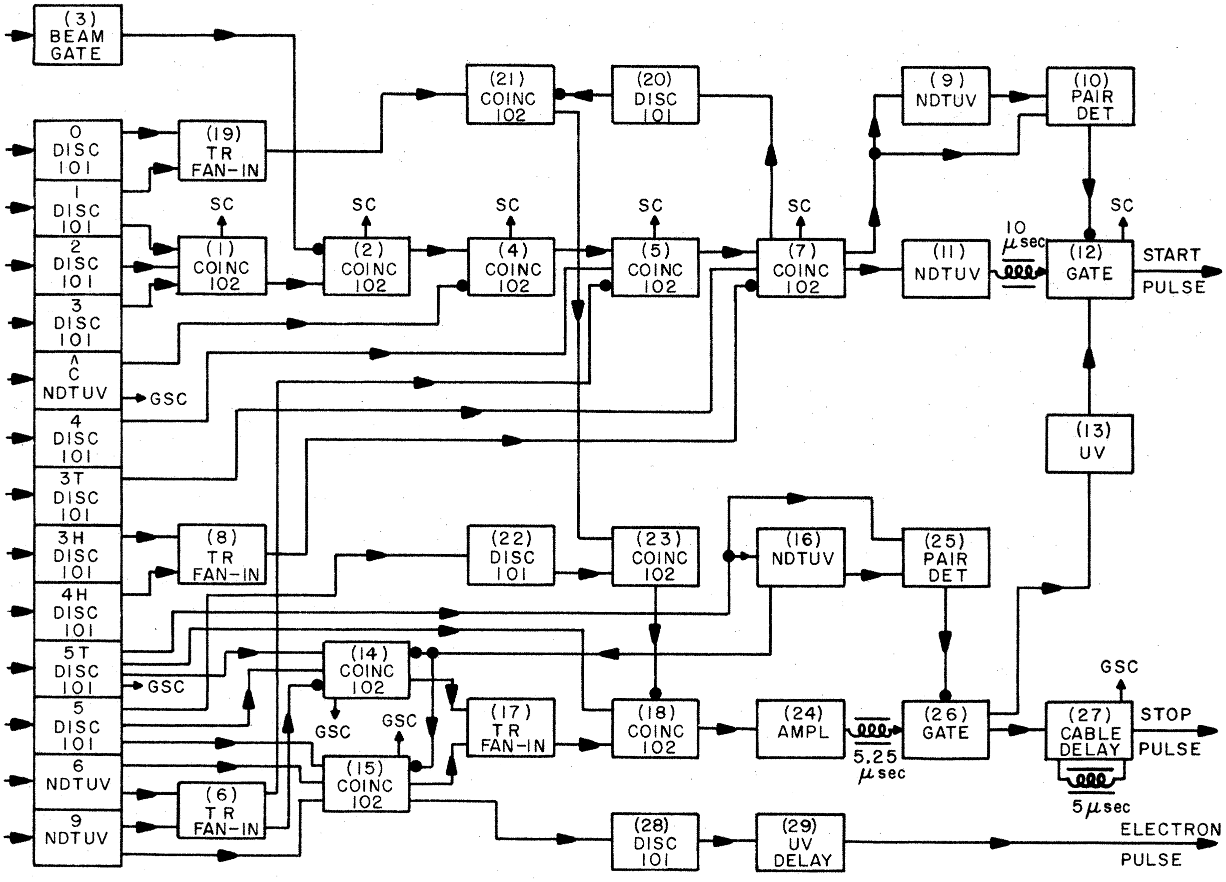

FIG. 4. Fast and slow logic. The numbers 101 and 102 on circuits refer to Chronetics discriminators and coincidence circuits, respectively, NDTUV stands for no-dead-time univibrator, TR for tunnel rectifier, SC for scaler, and GSC for scaler gated off by the beam gate during periods of high beam intensity. The sumbols 0 through 9 and C̆ on the discriminators refer to counter numbers.

plementary logic provided that either neutron or γ-ray pulse heights could be selected by means of the PSD pulse.

3. *Randoms Tests*

Randoms tests on the digital timing system were performed at frequent intervals using two well-separated counters, each placed near a radioactive source. The outputs of these counters were used to simulate start and stop events going into the digital timing system. In run III, the rms structure per channel was established to be less than 0.0025 for the 100-MHz data and less than 0.000 96 for the 50-MHz data. In addition, the number of counts per channel in the randoms tests and the various scaler readings were in agreement with the values predicted based on the various dead-time requirements imposed.

D. Positive-Beam Run

Electrons from muon decay produced bremsstrahlung γ rays in the target and in nearby shielding. These γ rays caused photonuclear reactions in the carbon of the liquid scintillant in counter 5, with the emission of neutrons or protons. These neutrons and protons were indistinguishable from neutrons and recoil protons due to muon capture in the target. Since the decay electrons had a negative asymmetry, and since the bremsstrahlung γ rays exhibited some fraction of this asymmetry, any bremsstrahlung γ rays identified as capture neutrons contributed a false negative component to the asymmetry. In order to determine the magnitude of this effect, a run was made using a positive beam. Positive muons were stopped in the target, and the number of decay electrons and the number of events identified as neutrons as a function of pulse height were measured. Since no positive muons were captured, all events identified as neutrons were associated with muon decay. The calcium target was used for this run because, having the highest Z of the three targets, it provided the highest production of bremsstrahlung quanta per decay electron. The ratio of the number of neutron-identified events to the number of decay electrons in the positive-beam run was compared to this ratio for the negative-beam runs. In the positive-beam run, only the lowest-energy neutron bin showed a statistically significant number of neutron-identified events. The case of silicon was used for evaluating the importance of neutron-identified γ rays because silicon had the lowest ratios of neutrons to decay electrons in the negative-beam runs, and therefore represented the worst case. In silicon, approximately 1.7% of the neutron-identified events in the lowest-energy bin were due to decay electron bremsstrahlung. This percentage is negligible compared to other sources of error.

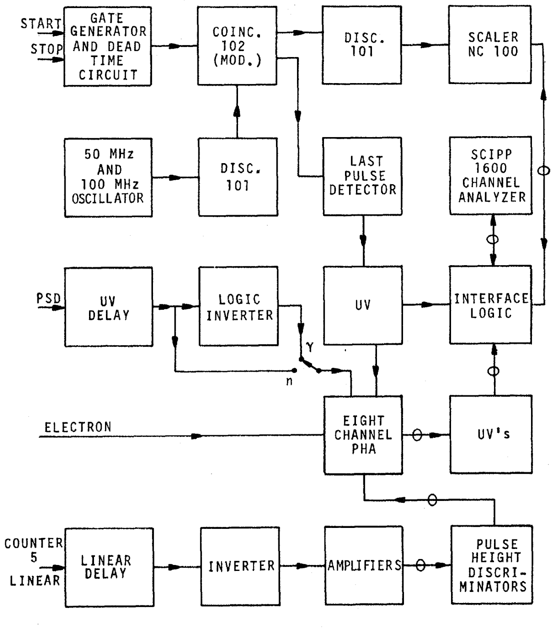

FIG. 5. Two-dimensional analyzer.

E. Experimental Procedure

Prior to each run, the assembled electronics was tested using electronically simulated events and using events simulated with counters and sources. Randoms tests were run and detailed electronics tests were made at least once a week.

In run II, 7×10^8 muons were stopped in each of the three targets. The average muon stopping rate was 2000 per second. In run III, 2×10^9 muons were stopped in each of the two targets used, at an average rate of 5000 per second. The total muon intensity was 40 000 muons per second, but only 5000 per second of this number were accepted because of the relatively thin target used, the dead-time requirements, and other requirements used to improve the quality of the data.

The C magnet was operated at a field of 415 g for the calcium and sulfur targets, and at a field of 207 g for the silicon target. These fields produced approximately two precessions per bound muon lifetime.

The time interval covered by the digital timing system was 2 μsec for the calcium and sulfur targets, and 4 μsec for the silicon target. The zero time was displaced so that approximately 0.25 μsec of negative time was observed.

Measurements were made of the γ-ray spectrum, as well as of the neutron spectrum. The number of neutron and γ events per muon stop were comparable in the lowest-pulse-height bins, but the γ spectrum fell off much more rapidly than did the neutron spectrum with increasing pulse height. In run III, the asymmetry observed for γ rays in the next to lowest-pulse-height bin, using the silicon target, was -0.150 ± 0.084 times the maximum possible asymmetry.

A measurement was made during run II with a carbon target, and with the electronics arranged so that decay electrons were distributed into the pulse-height bins. These data showed a negative asymmetry which was generally increasing in magnitude as the pulse height increased. The results are shown in Table I. The values of χ^2 obtained for this analysis, and also for the analysis of the sum of the data in the seven pulse-height bins, are excellent.

The asymmetry data were obtained from measurements made with the pulse-shape discriminator set so that a negligible number of γ rays were identified as neutrons. The spectrum data were taken together with a pulse-shape spectrum for each pulse-height interval, with the pulse-shape discriminator set for optimum separation of γ rays and neutrons. Corrections were then made for neutrons identified as γ rays and for γ rays identified as neutrons.

In run II all data were taken with the precession field in one direction and for one set of pulse-height intervals. In run III data were taken with alternating field directions and for two sets of pulse-height intervals, one corresponding to run II for the range 7.73 MeV < proton recoil energy < 52.53 MeV and the other for the region 4.25–7.73 MeV.

III. NEUTRON ASYMMETRIES

A. Data Analysis

The asymmetry exhibited by the decay electron timing spectrum provided a measurement of the residual polarization of the muon in the atomic ground state of the atom in which the muon had become bound, since the asymmetry in the angular distribution of decays from completely polarized negative muons is known to be $-\frac{1}{3}$.[15] This polarization was less than unity because the initial polarization of the part of the beam used was less than unity and because the muon loses a substantial fraction of its initial polarization in the process of being captured into an atomic orbit.

In addition to the decay electrons from the target element, the decay electron timing spectra also exhibited flat random background and the decay electron background from lead and carbon. The lead background was due to muons stopping in the lead and tantalum shielding in the vicinity of the target, and the carbon background was due to muons stopping in the dead layer of the telescope anticoincidence counter, counter 9.

The form of the equation used in fitting the timing spectra of the decay electrons was $I(t)=Ce^{-R_1t}\times[1+A\cos(\omega t+\phi)]+Le^{-R_2t}+De^{-R_3t}+W$, where I is the number of events per unit time after a muon stop, t is time, C is the amplitude of real events, R_1 is the disappearance rate of muons in the target, A is the asymmetry in the angular distribution of the decay electrons, ω is the angular precession frequency of the muons, ϕ is the phase of the asymmetry and is determined by the direction of the muon beam polarization and the geometry of the apparatus, L is the amplitude of lead events, R_2 is the disappearance rate of muons in lead, D is

TABLE I. Carbon decay electron asymmetry.

Bin	Minimum pulse height, electron (MeV)	Maximum pulse height, electron (MeV)	Asymmetry	Asymmetry error	χ^2 standard deviations above expected
	Sum of bins 2–8		−0.0502	0.0019	−0.73
2	3.5	6.0	−0.0397	0.0047	+0.52
3	6.0	9.0	−0.0288	0.0045	+1.55
4	9.0	12.0	−0.0366	0.0049	−1.26
5	12.0	16.0	−0.0487	0.0045	−0.84
6	16.0	20.0	−0.0641	0.0045	−0.19
7	20.0	25.0	−0.0737	0.0048	−0.49
8	25.0	40.0	−0.0916	0.0095	−0.00

the amplitude of carbon events, R_3 is the disappearance rate of muons in carbon, and W is the amplitude of the random background. The decay electrons from lead and carbon are also expected to exhibit asymmetries, but the number of lead and carbon events was sufficiently small that their asymmetries were not statistically significant, and were therefore omitted. The coefficients C, R_1, A, ω, ϕ, L, D, and W were fitted to the data by a least-squares calculation. R_2 and R_3 were taken from the literature[16] because their values were not well determined in this experiment due to the small number of lead and carbon background events.

The values of C, A, L/C, D/C, W/C, $1/R_1$, C/R_1, $\omega/2\pi$, and ϕ found for the decay electrons from each of the three target elements are presented in Table II. The values for run III are weighted averages of the field up and field down data. The number of degrees of freedom in the analysis was large, so that the number of standard deviations by which the observed value of χ^2 exceeded the expectation value was a good measure of the quality with which the equation fitted the data. This number of standard deviations is also given in the table.

All background to real amplitude ratios were evaluated at zero time. The error on the disappearance rate R_1 was considerably larger than it would have been if the lead and carbon background terms were omitted from the analysis. The ratio C/R_1 is approximately equal to the number of real events observed. The observed values of ω were in good agreement with those expected, based on the measured magnetic fields. The value of ϕ agreed well with that expected from the geometry.

The timing spectra of the neutrons were fitted by an equation similar to that used for the decay electrons. In the case of the neutrons, however, the random background was modulated with a sine wave having the frequency of the synchrocyclotron at the time the protons struck the internal target. This modulation was not visible in the electron timing spectra because most of the electron background arose from decays of muons stopping in the absorber. The lifetime of the muons in the absorber was sufficiently long compared to the period of the cyclotron radio frequency that the modulation was averaged out. The capture rate in carbon was sufficiently low and the random background was sufficiently high that the neutron background from carbon was not statistically significant. The carbon term was therefore deleted from the analysis.

The form of the equation used in fitting the timing spectra of the muon capture neutrons was

$$I(t)=Ce^{-R_1 t}[1+A\cos(\omega t+\phi)]+Le^{-R_2 t}+W[1+A_1\cos(\omega_1 t+\phi_1)]\ ,$$

where the repeated symbols have the same meanings as in the equation used in fitting the decay electron spectra. A_1 is the fractional radio frequency modulation amplitude, ω_1 is the angular

TABLE II. Decay electron asymmetry results.

	Run II Si	Run III Si	Run II S	Run II Ca	Run III Ca
C, real-event amplitude (counts/bin)	352 599 ± 304	1 536 539 ± 1.433	140 486 ± 282	122 112 ± 145	598 209 ± 581
A, asymmetry	−0.041 69 ± 0.000 43	−0.042 27 ± 0.000 24	−0.029 99 ± 0.000 56	−0.033 99 ± 0.000 79	−0.032 69 ± 0.000 38
L/C, lead-to-real amplitude ratio	0.0339 ± 0.0017	0.0125 ± 0.0025	0.0287 ± 0.0022	0.0333 ± 0.0025	−0.0096 ± 0.0034
D/C, carbon-to-real amplitude ratio	0.0076 ± 0.0006	0.0117 ± 0.0015	0.0082 ± 0.0026	0.0125 ± 0.0010	0.0161 ± 0.0019
W/C, random-to-real amplitude ratio	0.0038 ± 0.0001	0.0187 ± 0.0002	0.0070 ± 0.0012	0.0050 ± 0.0005	0.0150 ± 0.0008
$1/R_1$, lifetime (nsec)	756.0 ± 6.9	750.0 ± 1.1	555.8 ± 16.7	333.5 ± 4.5	330.0 ± 0.8
C/R_1, real events observed	13 326 000	57 619 000	7 809 000	4 072 000	19 741 000
$\omega/2\pi$, precession frequency (MHz)	2.879 ± 0.011	3.025 ± 0.001	5.677 ± 0.033	5.668 ± 0.056	5.993 ± 0.007
ϕ, precession phase (deg)	113.46 ± 0.58	85.48 ± 0.48	110.15 ± 1.05	107.95 ± 1.31	74.86 ± 1.16
χ^2, number of standard deviations high	+2.42	+1.53	+1.96	+0.10	+1.63

TABLE III. Neutron asymmetry results for silicon.

Element	$E_{\min}$ (MeV)	$E_{\max}$ (MeV)	C Real amplitude (cts/bin)	A asymmetry	L/C lead to real	W/C random to real	C/R_1 real events	A_1 rf amplitude	No. standard deviation in χ^2
Run II	7.73	11.49	9634 ± 26	+0.0038 ± 0.0029	+1.00 ± 0.02	0.080 ± 0.001	364 107	0.07 ± 0.01	+0.69
Silicon	11.49	15.62	3658 ± 17	+0.0237 ± 0.0049	+0.72 ± 0.04	0.110 ± 0.001	138 242	0.10 ± 0.01	+0.06
	15.62	19.54	1357 ± 11	+0.0456 ± 0.0085	+0.78 ± 0.07	0.173 ± 0.002	51 302	0.11 ± 0.01	+1.18
	19.54	24.55	664 ± 9	+0.0292 ± 0.0133	+0.75 ± 0.10	0.295 ± 0.005	25 108	0.11 ± 0.01	+2.48
	24.55	29.41	232 ± 6	+0.0498 ± 0.0258	+0.63 ± 0.19	0.54 ± 0.02	8759	0.13 ± 0.01	+0.77
	29.41	35.34	115 ± 5	−0.0161 ± 0.0427	+0.42 ± 0.30	0.94 ± 0.04	4363	0.09 ± 0.01	+0.07
	35.34	52.53	69 ± 6	+0.1043 ± 0.0763	−0.61 ± 0.50	2.16 ± 0.19	2612	0.11 ± 0.01	+0.29
Run III	4.25	7.73	974 ± 8	−0.0054 ± 0.0087	+0.26 ± 0.05	0.048 ± 0.001	36 532		+0.18
Silicon	7.73	11.49	38764 ± 49	+0.0063 ± 0.0014	+0.22 ± 0.01	0.063 ± 0.000	1 453 611		+3.53
	11.49	15.62	13455 ± 28	+0.0183 ± 0.0024	+0.20 ± 0.01	0.054 ± 0.000	504 549		+0.34
	15.62	19.54	4361 ± 16	+0.0381 ± 0.0042	+0.21 ± 0.02	0.051 ± 0.001	163 533		+0.12
	19.54	24.55	2131 ± 11	+0.0448 ± 0.0061	+0.18 ± 0.03	0.067 ± 0.001	79 910		−0.13
	24.55	29.41	669 ± 7	+0.0427 ± 0.0114	+0.25 ± 0.06	0.107 ± 0.002	25 072		+0.12
	29.41	35.34	251 ± 5	+0.0395 ± 0.0199	+0.14 ± 0.09	0.180 ± 0.005	9397		−0.14
	35.34	52.53	129 ± 4	−0.0016 ± 0.0324	−0.03 ± 0.15	0.426 ± 0.015	4837		+0.66

radio frequency, and ϕ is the phase of the radio frequency. The value of R_2 used for the decay electron spectra was used in fitting the neutron spectra. The values of R_1 and ω found for the electron spectra were used in this equation. At first, the value of ϕ was fitted. After it was established that the value obtained was within statistical accuracy equal to the value obtained for the electrons, the electron value, which was much more accurate, was used as fixed input for the neutrons. The values of C, A, L, W, A_1, ω_1, and ϕ_1, were fitted to the data by a least-squares calculation. Due to the different beam stretcher used in run III, A_1 was found to be insignificant, and it was deleted from the analysis.

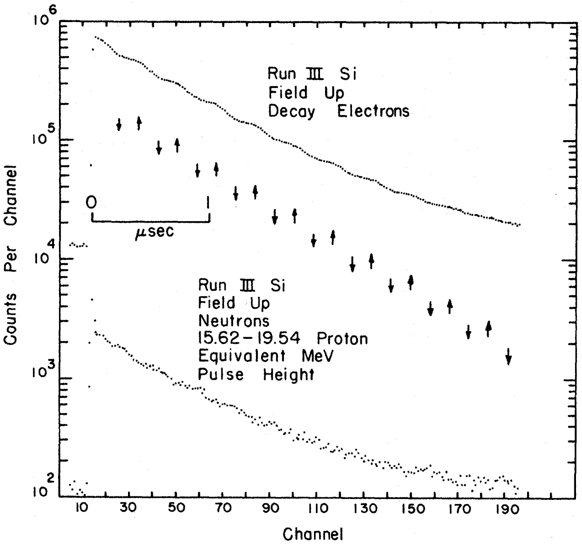

FIG. 6. Time spectra in silicon for decay electrons and for neutrons following muon capture.

The average value found for $\omega_1/2\pi$, the radio frequency of the synchrocyclotron, was 20.45 MHz for the three targets in run II. All radio frequency phases were near 0°, as expected. Sample results for Si of the values found for C, A, L/C, W/C, C/R_1, A_1, and the number of standard deviations by which the observed value of χ^2 exceeded the expected value are presented in Table III. Run III values are weighted averages of field up and field down results. These results were generally in excellent agreement. The energies of recoil protons corresponding to the lower and upper pulse-height limits of each bin are given in columns 2 and 3, respectively, of the table. The number of standard deviations by which the observed value of χ^2 exceeded the expectation value is given in column 10. Note that in general they are well within acceptable limits.

Two typical timing spectra are shown in Fig. 6. The decay electron spectrum and the neutron spectrum corresponding to 15.62- to 19.54-MeV recoil protons are shown for the silicon target. Arrows indicate the fitted positions of the electron asymmetry peaks. The gradual curvatures of the spectra are due to random background. A careful study of the raw neutron data with the naked eye will convince one that the sinusoidal component of the curve is ~180° out of phase with the more clearly observed electron data. We feel that it is important to be convinced of this before proceeding to

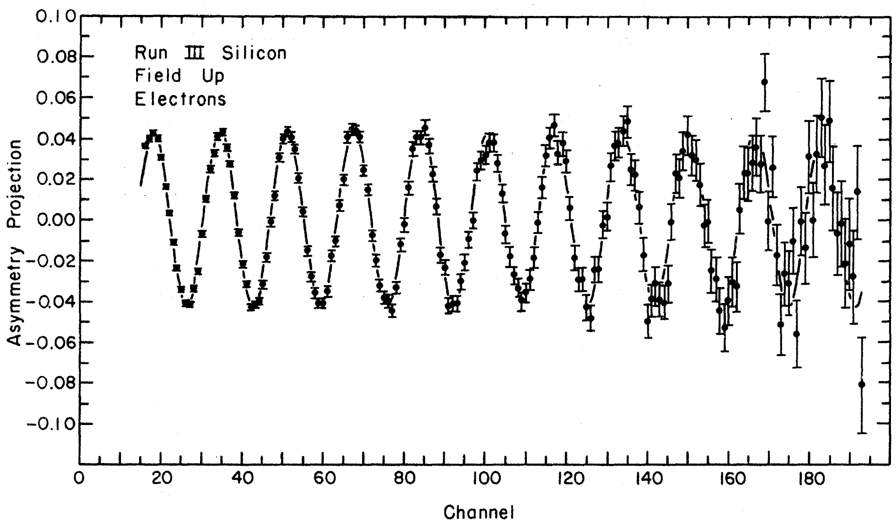

FIG. 7. Extracted sinusoidal component of time spectrum in silicon for decay electrons.

the results of a sophisticated least-squares analysis.

The sinusoidal component of the timing spectrum becomes more readily visible when this component is extracted from the spectrum. The extracted sinusoidal component for the run III silicon decay electron data taken with the precession field up, together with the fitted function $A\cos(\omega t+\phi)$, is shown in Fig. 7.

The extracted sinusoidal component for the same silicon decay electron data, but with the use of an appropriately weighted five channel averaging of the data, is shown in Fig. 8. The corresponding extracted sinusoidal component for silicon neutrons with pulse heights between 15.62 and 19.54 proton equivalent MeV is shown in the same figure. The excellent quality of the fits both to electron and neutron timing spectra is readily apparent.

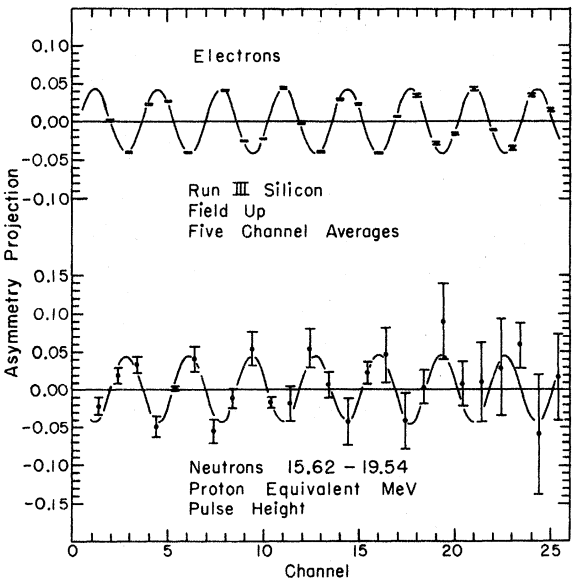

FIG. 8. Sample extracted sinusoidal component of time spectra in silicon for decay electrons and for neutrons following muon capture.

B. Asymmetry Corrections

The measured electron asymmetry was used to determine the residual polarization of the muons in the atomic ground state, and the quoted final neutron asymmetries are normalized to the residual polarizations. Since the electron and neutron asymmetries were measured simultaneously, this ratio was not subject to any effect due to variations in the beam polarization.

It was calculated that a target thickness of 4.0 g/cm^2 would not scatter the decay electrons enough to cause a significant reduction in the measured

TABLE IV. Thin-target electron asymmetries.

Target element	Target thickness (g/cm^2)	Asymmetry	Asymmetry error
Calcium	4.0	−0.0340	0.0008
	2.0	−0.0309	0.0037
	1.0	−0.0284	0.0054
Sulfur	4.0	−0.0300	0.0006
	2.0	−0.0288	0.0026
	1.0	−0.0291	0.0043

TABLE V. Normalized neutron asymmetry results.

Target element	Recoil proton energy, min. (MeV)	Recoil proton energy, max. (MeV)	Fraction of max. allowable asymmetry	Error in asymmetry	Asymmetry, standard deviations from zero
		A. Differential energy bins			
Run III Silicon	4.25	7.73	−0.053	0.078	−0.68
	7.73	11.49	+0.050	0.011	+1.58
	11.49	15.62	+0.144	0.019	+7.72
	15.62	19.54	+0.300	0.033	+9.17
	19.54	24.55	+0.353	0.048	+7.38
	24.55	29.41	+0.340	0.090	+3.80
	29.41	35.34	+0.317	0.157	+2.02
	35.34	52.53	−0.019	0.255	−0.07
Run II Sulfur	7.73	11.49	+0.096	0.034	+2.80
	11.49	15.62	+0.172	0.058	+2.98
	15.62	19.54	+0.272	0.105	+2.60
	19.54	24.55	+0.437	0.155	+2.83
	24.55	29.41	+0.100	0.310	+0.32
	29.41	35.34	+0.407	0.540	+0.75
	35.34	52.53	−0.629	1.074	−0.59
Run III Calcium	4.25	7.73	−0.037	0.025	−1.48
	7.73	11.49	+0.059	0.017	+3.60
	11.49	15.62	+0.170	0.030	+5.66
	15.62	19.54	+0.336	0.049	+6.79
	19.54	24.55	+0.273	0.071	+3.86
	24.55	29.41	+0.184	0.127	+1.45
	29.41	35.34	+0.229	0.224	+1.02
	35.34	52.53	+1.097	0.370	+2.96
		B. Integral energy bins[a]			
Run III Silicon	4.25		0.101	0.009	11.40
	7.73		0.103	0.009	11.56
	11.49		0.205	0.015	13.45
	15.62		0.315	0.026	12.35
	19.54		0.339	0.040	8.39
	24.55		0.304	0.075	4.07
	29.41		0.225	0.134	1.68
	35.34		−0.019	0.255	−0.08
Runs II and III Silicon	4.25		0.101	0.008	12.65
	7.73		0.103	0.008	12.79
	11.49		0.210	0.014	15.35
	15.62		0.316	0.023	13.70
	19.54		0.323	0.037	8.79
	24.55		0.303	0.068	4.44
	29.41		0.203	0.122	1.67
	35.34		0.110	0.235	0.47
Run III Calcium	4.25		0.080	0.012	6.66
	7.73		0.116	0.014	8.41
	11.49		0.224	0.023	9.55
	15.62		0.310	0.038	8.22
	19.54		0.272	0.059	4.61
	24.55		0.269	0.106	2.54
	29.41		0.462	0.192	2.41
	35.34		1.097	0.370	2.97

[a] Asymmetries for neutrons with pulse heights exceeding the specified recoil proton energy equivalent. Bins included in each average are statistically weighted.

asymmetry. This was confirmed by measurements using targets with effective thicknesses of 2.0 and 1.0 g/cm^2, in addition to the normal 4.0-g/cm^2 targets. The results of these measurements are presented in Table IV.

C. Neutron Asymmetry Results

The measured neutron asymmetries have been divided by the polarization of the muons in the atomic ground state, as determined from the electron asymmetries. These fractions are presented in Table V A for run III and the *S* data of run II. Note again that the energy bins in this table are for proton recoil energies. The numbers of standard deviations by which these asymmetries differ from zero are also given in the table. The observed asymmetries are very close to zero for low-energy neutrons, and all three targets exhibit an asymmetry which, in general, becomes increasingly positive as the neutron energy increases. The fractions of the maximum allowable asymmetries are shown as a function of median bin pulse height for the three targets in Fig. 9. The data for field up and field down of run III are in excellent agreement, therefore the results quoted are averages of the two. The integral asymmetries as a function of recoil-proton threshold energy are given in Table V B for Ca and Si in run III and for the weighted average of runs II and III for Si.

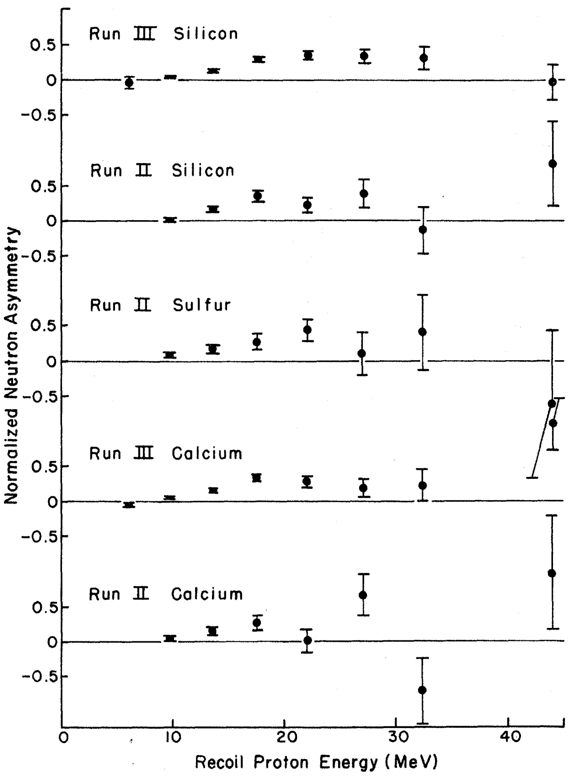

FIG. 9. Neutron asymmetry vs recoil-proton equivalent energy. The asymmetry is normalized to unity muon polarization.

Since previous experiments have obtained large negative neutron asymmetries, a thorough study was made of mechanisms that could induce a false positive asymmetry. No particles emitted from the target, other than neutrinos, are expected to exhibit a positive asymmetry. Nuclear γ rays are isotropic, and decay electrons and their associated bremsstrahlung γ rays exhibit negative asymmetries. A small negative asymmetry was observed for γ rays, as has been described earlier.

The possibility that the random background contains a sinusoidal component with a frequency near the precession frequency, or that the digital timing system contains such a component, is ruled out by use of both directions of the precession field and by the randoms tests. The asymmetries obtained using two directions of the precession field were in agreement with each other, and the randoms tests exhibited no such structure. Instrumental effects due to the finite resolving time of the fast electronics were established to be negligible.

Due to the small number of large-pulse-height neutron events compared to the number of large-pulse-height decay electron events, a relatively small dead time in an anticoincidence counter used to distinguish electrons from neutrons, coupled with a pulse-shape discriminator which identified a small fraction of electrons as neutrons, would induce a significant false negative asymmetry. In both runs II and III anticoincidence pulses were combined in a dead-timeless fashion. In addition, the pulse-shape discriminator was carefully checked at all pulse heights of interest. The analysis programs were checked using randomized artificial data to confirm that the programs were yielding correct values and errors.

In summary, no mechanisms capable of causing significant false asymmetries, either positive or negative, have been found in this experiment.

The data from run III had sufficient statistical significance to make it practical to unfold the asymmetry as a function of pulse height to obtain the asymmetry spectrum as a function of neutron energy. This was done by subtracting the contribution to the asymmetry at each pulse height due to neutrons of higher energy. The contributions due to higher-energy neutrons were determined from the pulse-height spectrum, the asymmetries observed at higher pulse heights, and the pulse-height response of counter 5 as a function of neutron energy. The procedure for determining the pulse-height response of the neutron detector is discussed in Sec. IV.

The neutron asymmetry as a function of neutron energy for the run III silicon and calcium is shown in Table VIA and Fig. 10. Table VIB gives the integral asymmetries as a function of neutron energy threshold. Figure 10 also shows the results of Sculli[17] for the neutron asymmetry as a function of energy for a calcium target.

D. Discussion of Asymmetry Results

Early calculations of the neutron asymmetry[2] predicted negative asymmetries around −0.4. More recently there have been three important calculations in this field, all tending to move the predicted asymmetry into closer agreement with the data of this experiment. First, Klein, Neal and Wolfenstein,[6] using a Fermi-gas model of the nucleus, showed that including first-order relativistic

TABLE VI. Neutron asymmetries vs energy.

Target element	Neutron energy, min. (MeV)	Neutron energy, max. (MeV)	Fraction of max. allowable asymmetry	Error in asymmetry	Asymmetry, standard deviations from zero
		A. Differential energy bins			
Run III Silicon	4.25	7.73	−0.117	0.107	−1.10
	7.73	11.49	−0.026	0.023	−1.14
	11.49	15.62	+0.038	0.041	+0.92
	15.62	19.54	+0.270	0.056	+4.81
	19.54	24.55	+0.349	0.091	+3.84
	24.55	29.41	+0.387	0.165	+2.35
	29.41	35.34	+0.406	0.190	+2.14
	35.34	52.53	−0.019	0.255	−0.07
Run III Calcium	4.25	7.73	−0.087	0.034	−2.55
	7.73	11.49	−0.033	0.034	−0.96
	11.49	15.62	+0.081	0.054	+1.49
	15.62	19.54	+0.385	0.097	+3.97
	19.54	24.55	+0.372	0.141	+2.63
	24.55	29.41	+0.095	0.212	+0.45
	29.41	35.34	−0.096	0.311	−0.31
	35.34	52.53	+1.097	0.370	+2.96
		B. Integral energy bins [a]			
Run III Silicon	4.25		0.002	0.047	0.05
	7.73		0.091	0.020	4.50
	11.49		0.181	0.031	5.84
	15.62		0.307	0.046	6.70
	19.54		0.341	0.072	4.77
	24.55		0.332	0.113	2.95
	29.41		0.285	0.154	1.85
	35.34		−0.019	0.255	−0.07
Run III Calcium	4.25		0.012	0.023	0.53
	7.73		0.105	0.030	3.50
	11.49		0.209	0.046	4.56
	15.62		0.333	0.074	4.53
	19.54		0.292	0.107	2.73
	24.55		0.216	0.160	1.35
	29.41		0.338	0.239	1.41
	35.34		1.097	0.370	2.97

[a] Asymmetries for neutrons with energies exceeding the specified values. Bins included in each average are weighted by the energy spectrum.

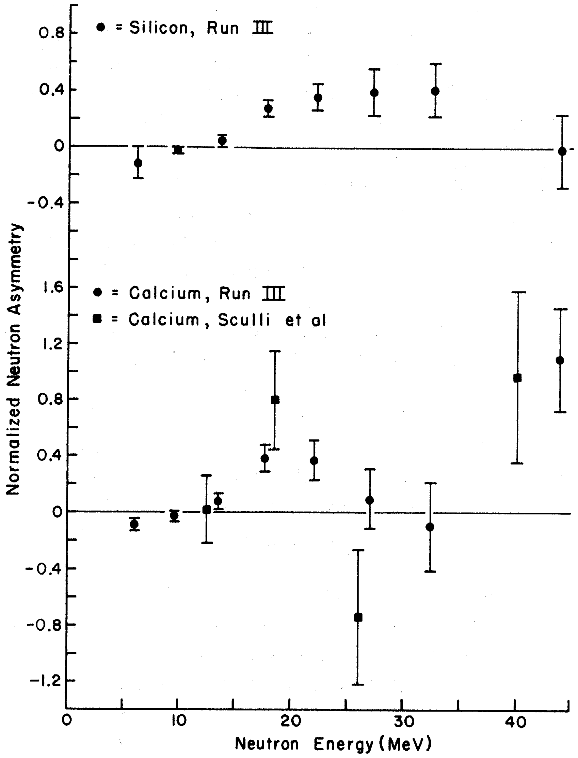

FIG. 10. Neutron asymmetry vs neutron energy for run III. The asymmetry is normalized to unity muon polarization.

terms in the effective Hamiltonian reduced the magnitude of the still negative asymmetry. Second, Bogan,[7] using the same Hamiltonian, but with a nuclear shell model, obtained positive (although small) asymmetries. Thus, both the relativistic terms and the nuclear model were shown to be important. Finally, Piketty and Procureur[8] have shown that second-order relativistic terms are important in the Hamiltonian. Their results using a nuclear shell model are in rough agreement with these data, although still tending to be low. They have also shown that neither spin-orbit nor final-state interactions affect markedly the neutron asymmetries, while the latter, as expected, do reduce the absolute level of the spectra significantly. Because of the uncertainties in the nuclear model especially with regard to higher-order relativistic corrections, there is still considerable uncertainty connected with these predictions. They are still quite significant, however, in showing that rough agreement with the data can be achieved with a plausible model, and that no bizarre and unusual effect need be invoked to bring theory into agreement with experiment. Examples of the predictions are shown in Fig. 11.

The asymmetry of neutrons due to the capture of negative muons in various nuclei has been measured as a function of pulse height by a number of authors.[18] All of these measurements were made using techniques similar to the one used in this experiment. One difference was the method used to distinguish γ rays from neutrons. The experiment by Coffin, Sachs, and Tycko[19] did not distinguish γ rays from neutrons. Experiments by Baker

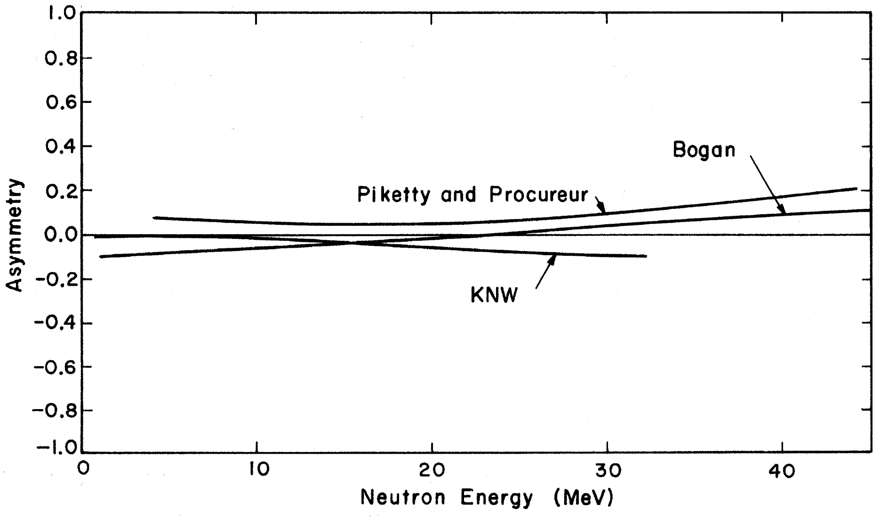

FIG. 11. Sample theoretical predictions of the asymmetries in Ca taken from Klein, Neal, and Wolfenstein (Ref. 6) (KNW), Bogan (Ref. 7), and Picketty and Procureur (Ref. 8) (PP).

and Rubbia[20] and by Evseev *et al.*[21] used sandwich counters and the fact that recoil protons have shorter ranges than Compton electrons to distinguish neutrons from γ rays. All of the other experiments used pulse-shape discrimination to distinguish neutrons from γ rays.

A second difference was the method of measuring the time spectra. One method used was that of a fixed time window and reversing the precessing field to change the sense of the muon precession. The neutron asymmetry was determined from the ratio of the counts with the muon polarization vector pointing toward and away from the neutron detector. This method was used by Coffin, Sachs, and Tycko,[19] by Baker and Rubbia,[20] and by Evseev *et al.*[22] Reversal of the magnetic field has the disadvantage that effects of the field reversal on the gain of the neutron detector photomultiplier must carefully be taken into account.

The other three methods of measuring the timing spectrum are similar to each other, since they measure the time between a stopping muon and a neutron. The devices used are: (1) a pulse-height converter and a pulse height analyzer, (2) an oscilloscope and film, or (3) a digital timing system. The last of these methods has the advantage that its associated nonlinearity is negligibly small, although the nonlinearity of the other two methods can be measured and taken into account in the analysis of the data.

The results of the previous neutron asymmetry experiments are presented in Fig. 12. The targets used and the methods of measuring the asymmetries used by each group are given in the legend of this figure. The asymmetries are plotted as a function of the neutron energy threshold, rather than as a function of the median bin energy, because many of the bins are integral rather than differential. Only the lowest two digital calcium values and the lowest two digital carbon values from the data of Anderson[23] are presented in differential form; all other points are integral. With the exceptions of the Anderson digital data, the calcium scope value of Evseev *et al.*[24] at 7.0 MeV, which point was obtained in a separate experiment, and the two values of Astbury *et al.*,[25] which points were obtained in separate experiments, the data represented by a point of one symbol are included in the data of all lower energy points having the same symbol.

If it is assumed that the asymmetry is not a sensitive function of the nucleus used, all of the data can be compared. The results of the present experiment are consistent with the results of Baker and Rubbia,[20] with the digital calcium results of Anderson,[23] and with the digital and scope carbon results of Anderson.[23] The results of the present experiment are inconsistent with Astbury *et al.*,[25] Telegdi,[26] Evseev *et al.*,[20] and with the scope calcium results of Anderson.[22]

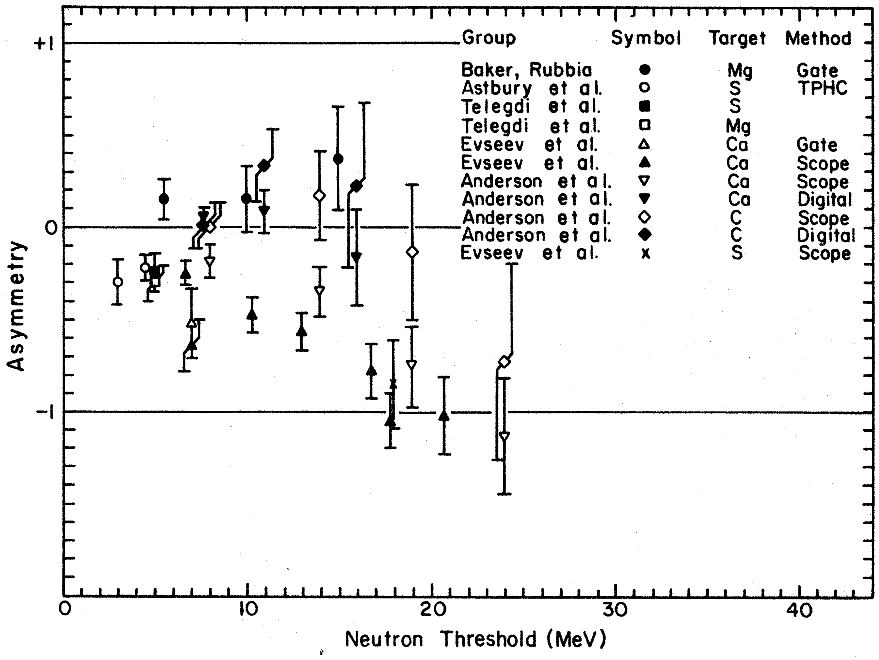

FIG. 12. Previous asymmetry results vs recoil-proton equivalent energy.

An experiment by Sculli[17] measured the neutron asymmetry directly as a function of neutron energy. The neutron energy was determined from the range and direction of the recoil proton in a thin-plate spark chamber. Their results for Ca are shown in Fig. 10, together with our run III calcium results. The agreement between the two experiments is good; a comparison of their four points with our nearest four points yields a χ^2 of 3.9. In addition, a comparison of our run II and run III results for the asymmetry as a function of pulse height yields good values of χ^2. The χ^2 for the seven corresponding silicon points is 6.5, and for the seven corresponding calcium points is 8.7. Each of the run II points is within 2 standard deviations of the corresponding run III point.

The extensive precautions observed in the present experiment, the agreement between the results of runs II and III using substantially different electronics, the agreement of our experiment with the experiment of Sculli,[17] using a totally different method, the agreement between the field up and field down results in run III, and the absence of any possible mechanism for inducing a false positive asymmetry lead to our great confidence that the results of the present experiment are correct.

It is encouraging that the asymmetries as a function of neutron energy predicted in Ref. 7 have forms similar to our data. However, the fact that the magnitude of our observed asymmetry is larger than that predicted is difficult to explain, as any interaction of the final-state nucleus with the direct neutron would be expected to reduce the observed asymmetry. It is hoped that further refinements of the theoretical calculation will eliminate this discrepancy.[27]

IV. NEUTRON ENERGY SPECTRA

The two-dimensional spectra discussed in the preceding section yielded time and pulse-height information about each event. Analysis of the timing spectra yielded the number of real events in each pulse-height interval. The number of real events per unit pulse height as a function of pulse-height interval yields a pulse-height spectrum. This section discusses the unfolding of the neutron energy spectrum from this pulse-height spectrum.

A. Pion-Capture Neutron Time of Flight

The pulse-height response of counter 5 to monoenergetic neutrons was determined by accumulating pulse-height spectra at various incident neutron energies. The neutron energies were determined by a narrow time window imposed on the time of flight of a neutron. The time of flight of the neutron was equal to the time between the stopping of a negative pion in the target and the detection of a neutron in counter 5. The accumulation of these pulse-height spectra is described in more detail in Appendix B.

The pulse-height spectrum which would result from a certain neutron energy spectrum may be described by $p_i = m_{ij} n_j$, where p_i is the number of pulses observed in the ith pulse-height interval, n_j is the number of neutrons emitted in the jth energy interval, and m_{ij} is a coefficient determined by the target and detector geometry and by the properties of the detector scintillant and photomultiplier. These equations can be represented in matrix form as $P = MN$. Since P is determined by the experiment, and if M is known, N, the energy spectrum of the neutrons emitted from the target, is given by $N = M^{-1}P$.

M cannot be determined directly from the pion-capture neutron measurements for a number of reasons. Principally, the number of neutrons emitted in each energy interval from the target is not known. In addition, the difference in the geometries of the detector with respect to the target in the pion-capture neutron measurement and in the main experiment caused a small change in the shapes of the pulse-height spectra and a large change in the solid angle. The finite width of the neutron time-of-flight window and the finite resolution of the timing system in the pion-capture neutron measurement also cause difficulties in determining M. As a result, it was necessary to perform two sets of Monte Carlo calculations to determine M.

B. Pion-Capture-Neutron Monte Carlo Calculations

The first set of Monte Carlo calculations performed simulated the pion-capture-neutron time-of-flight measurement in order to establish that the methods of calculation adequately simulated the experimental data.

A parallel beam of neutrons was assumed to be incident upon counter 5. The distance from the target to counter 5 was sufficient to make this a good approximation. The energy distribution of these neutrons was taken to be that obtained by folding the 2-nsec full width at half maximum resolution of the timing system into the 2-nsec time-of-flight window. The types of scattering in the scintillant which were considered were $n + p \to n + p$, $n + \mathrm{C} \to n + \mathrm{C}$, $n + \mathrm{C} \to n + \mathrm{C}^*_{4.433}$, $n + \mathrm{C} \to n + 3\,\mathrm{He}$, and $n + \mathrm{C} \to p + \mathrm{B}$. See Refs. 28 and 29 for cross-section data. Although only the first of these reactions produced appreciable scintillation light for neutron energies below 16 MeV, the other reactions were important because they caused a reduction of the neutron energy. The $n+C\rightarrow p+B$ reaction contributed appreciable scintillation light for neutron energies above 16 MeV. The deviation from S-wave scattering becomes significant for neutron energies above 13 MeV for elastic scattering from hydrogen and above 1 MeV for elastic scattering from carbon and was accounted for. It was assumed that inelastic scattering was isotropic in the center-of-mass system because differential scattering data for the inelastic processes were not sufficiently complete. In addition, it was assumed that the three α particles from the reaction $n+C\rightarrow n+3$ He have negligible velocity relative to each other. The relative amount of light produced by the recoil particle was computed from curves based on Birks's equation.[30] The curve for protons has been discussed in Appendix B. Curves were also computed for completely ionized C, He, and B using the value of the constant kB found for protons. Tracking of the neutron through the scintillant was terminated when the neutron escaped, when its residual energy was negligible, or after the reaction $n+C\rightarrow p+B$.

When the tracking of a neutron and the computation of the total light produced were completed, the photostatistics of the counter were also simulated, based on the measured 165 photoelectrons per electron equivalent MeV. The event was then analyzed, with and without photostatistics, by simulated pulse-height analyzers.

The pulse-height spectra obtained experimentally were compared to the calculated pulse-height spectra to substantiate the computations. At low neutron energies, the agreement was quite good. At neutron energies above 17.5 MeV, the $n+C\rightarrow p+B$ total cross section had not been measured, and it was necessary to work backwards and determine this cross section from the comparison of the experimental and calculated curves. This was possible because the highest-energy proton from the $n+C\rightarrow p+B$ reaction has several MeV less than the highest-energy proton from the $n+p\rightarrow n+p$ reaction, for incident neutrons of the same energy. The higher-energy edge of the spectrum could therefore be used as a vertical amplitude normalization in determining the $n+C\rightarrow p+B$ cross section. It was possible to obtain good agreement between the experimental and calculated shapes by suitable selection of this single cross section.

Smooth curves were fitted to the Monte Carlo spectra. Two typical curves of this type are shown in Fig. 13. The negative slope near channel 80 in the 32.36-MeV neutron spectrum is due primarily to $n+C\rightarrow p+B$ reactions.

C. Muon-Capture-Neutron Monte Carlo Calculations

After establishing the validity of the assumptions made in the Monte Carlo calculations by comparing the results of these calculations to measured pion-

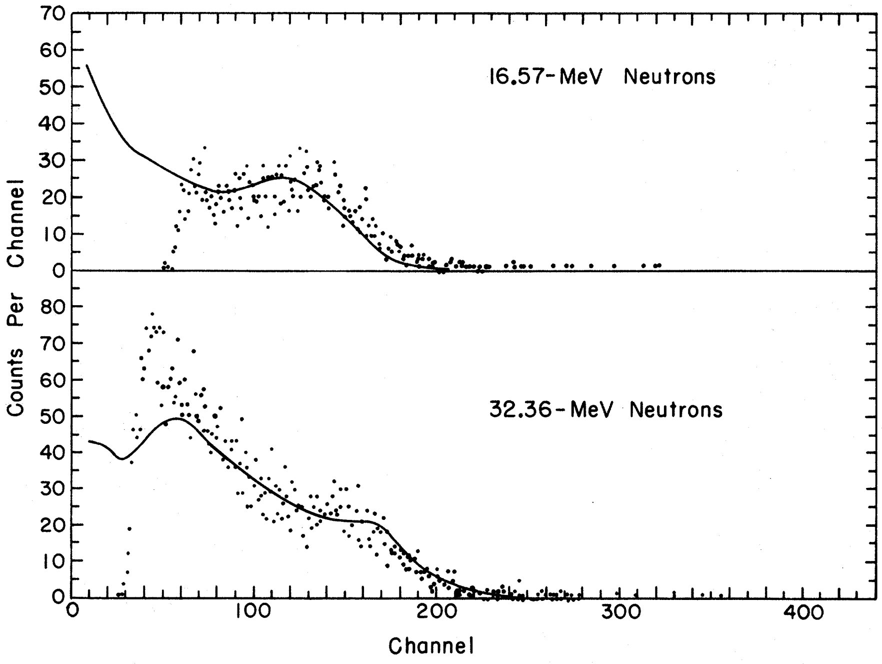

FIG. 13. Sample pulse-height spectra in counter 5 following π^- capture for neutrons of 16.57- and 32.36- MeV energy, respectively. Solid lines are fits to the Monte Carlo calculation.

capture-neutron pulse-height spectra, it was necessary to perform similar calculations to take account of the actual geometry used in the muon experiment. These calculations differed from those for pion-capture neutrons in that they used monoenergetic neutrons, the proper distribution of muons in the target, and the appropriate geometry of the counter with respect to the target.

The distribution of muons in the target was itself determined by a Monte Carlo calculation. A uniform parallel beam of muons was assumed to be incident on the first telescope counter. The measured momentum distribution of the beam was used in the calculations. The scattering of the muons in the counters and absorbers was taken into account to determine their stopping locations in the target.

Two typical Monte Carlo pulse-height spectra, with photostatistics, are shown in Fig. 14. The bump near the center of the lower spectrum is due to $n+\mathrm{C}\rightarrow p+\mathrm{B}$ reactions. Smooth curves have been fitted to the points.

The total number of neutrons which entered counter 5, whether or not they interacted, was recorded. The effective solid angle of counter 5 for decay electrons was determined from the ratio of this number to the total number of neutrons emitted. The effective fraction of unit sphere subtended was found to be 0.0710± 0.0001.

D. Neutron-Energy-Spectrum Calculation

The number of real events in each pulse-height bin has been determined from the analysis of the neutron asymmetry. The analysis of the digital timing spectra permitted the unambiguous subtraction of lead and random background. The neutron pulse-height spectra are presented, with statistical errors shown, in Fig. 15. These spectra represent the vector P discussed previously.

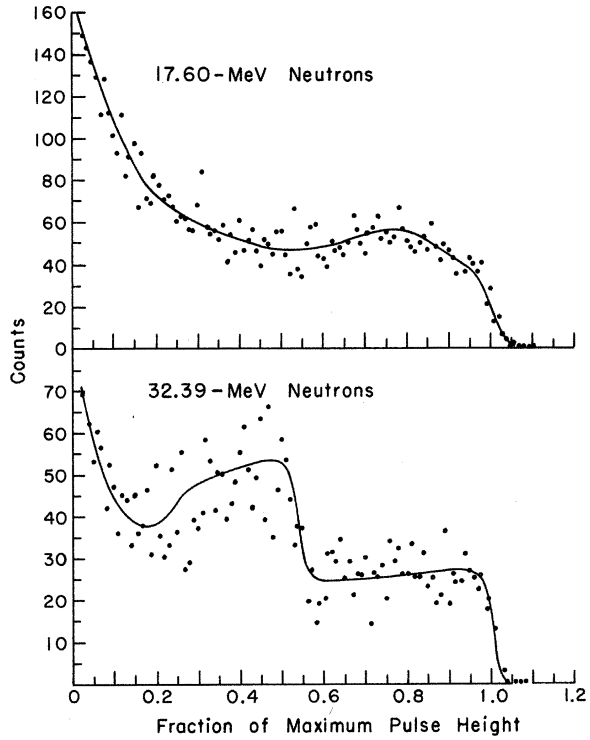

FIG. 14. Monte Carlo calculation for neutrons of 17.60- and 32.39-MeV energy, respectively, for the geometry of the muon-capture setup. Solid lines are smooth fits by eye to the Monte Carlo data.

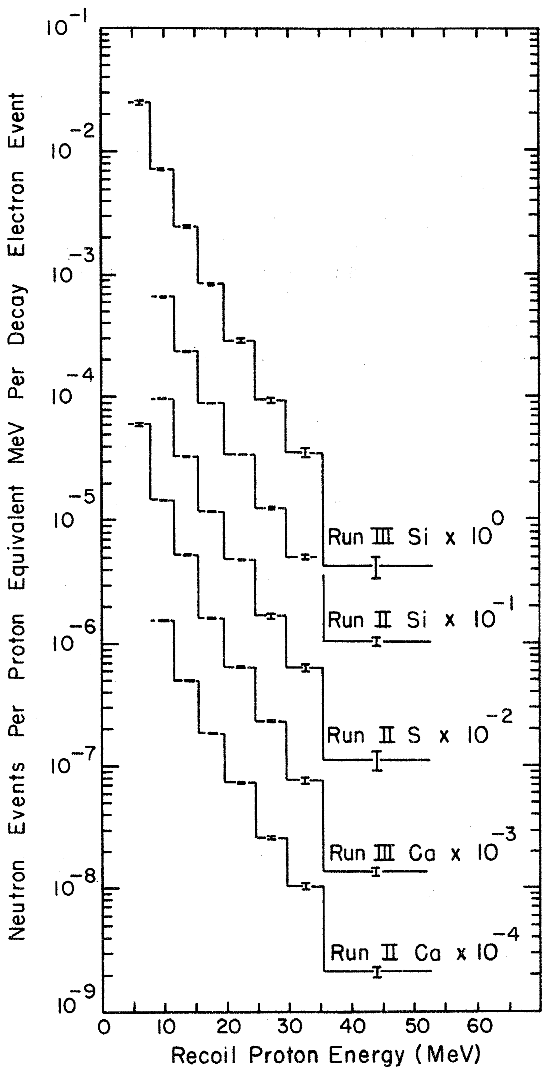

FIG. 15. Proton-recoil spectra from muon-capture neutrons.

Since there were statistical errors associated with the elements of M, as well as of P, the statistical errors on N were determined by numerical methods. In addition to the statistical errors, separate errors of 10% were assigned to each bin for: (1) uncertainties in neutron scattering cross sections, and (2) the effect of finite bin width.

The observed number of decay electrons was used to determine the number of muon stops in the target so as to normalize the neutron spectra. The effective fraction of unit sphere subtended at the target by counter 5 was determined as described previously. It was necessary to make a small correction to the number of decay electrons because the decay electrons lost energy by ionization and bremsstrahlung and because the pulse-height threshold for electron detection in counter 5 was nonzero.

Calculations were made of the effects of electron scattering on the fraction of decay electrons which registered in counter 5 using the detector geometry and the results of Huff[31] for the energy spectrum of the emitted electrons. The fraction of electrons not registered because of scattering and threshold effects was found to be approximately 0.08. The calculated spectra for electrons from the decay of free muons and bound muons, and the spectrum for decay electrons from bound muons after passing through the material between the center of the target and the scintillator of counter 5, are shown in Fig. 16. Factors not taken into account in the calculation were: (1) the loss by bremsstrahlung so that the residual energy was below threshold, (2) the loss of energy due to increases in path length from scattering and diagonal entry into counter 5, and (3) the loss of counts due to electrons escaping through the edges and front face of counter 5 before depositing the required threshold energy. An additional error of 10% has been assigned to the amplitude of the neutron energy spectrum due to these uncertainties in the normalization.

Note that no dead-time corrections had to be made in normalizing, as the dead-time circuitry affected the electrons and neutrons in an identical manner.

The normalized neutron energy spectra are presented in Fig. 17. The errors shown in the figure are the total errors, both statistical and systematic, and include the normalization error. The spectra are all consistent with a simple exponential dependence on E_n. For Si the constants are 7.6 MeV for run II and 6.5 MeV for run III. For S the constant is 7.3 MeV for run II and for Ca the constant is 7.2 MeV for run II and 6.6 MeV for run

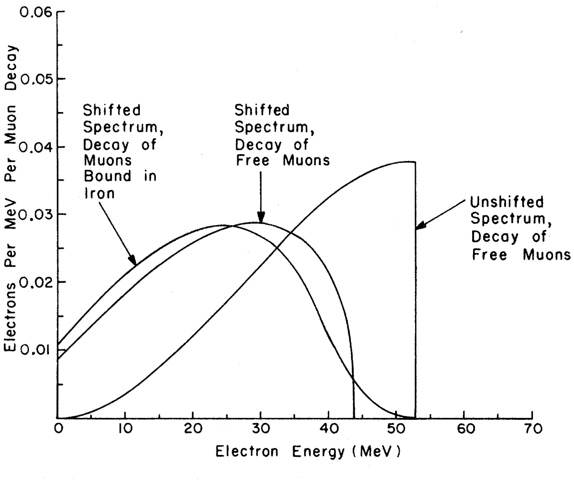

FIG. 16. Computed electron energy spectra in counter 5.

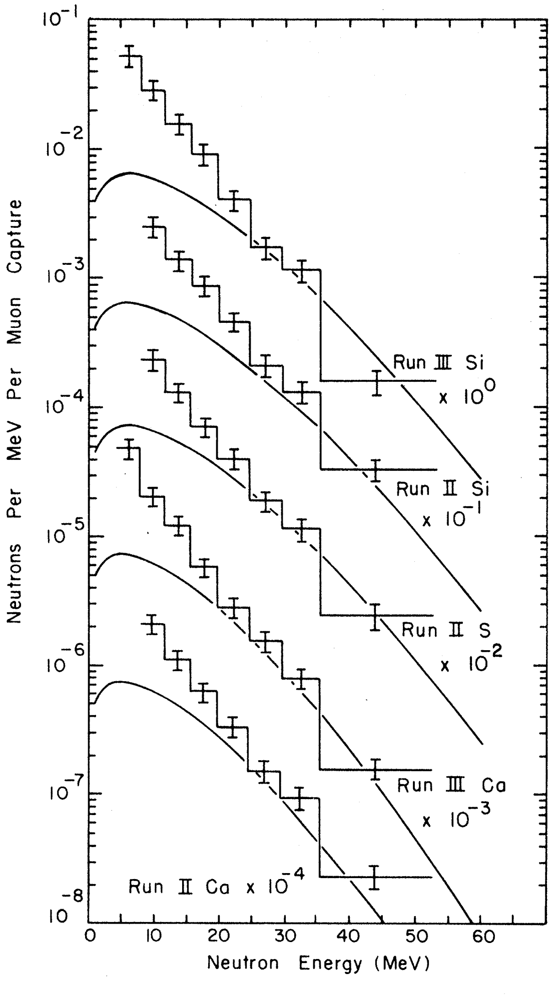

FIG. 17. Neutron energy spectra from muon capture. Curves are from the model of Bogan (Ref. 7).

III. These results are also presented in Table VII. The intergral spectra are also presented in this table. The integral spectra are the total number of neutrons per muon capture emitted with energy greater than the lower-energy limit of the associated bin. The errors on the integral spectra have been computed assuming that all individual bin errors are completely independent. The errors quoted on the integral spectra are thus slightly larger than the actual errors. Note that the results of the two runs on Si and Ca are in good agreement.

Since the neutron energy spectrum falls off rapidly with increasing energy, the probability of detecting two neutrons emitted following a single muon capture and identifying these as a single higher-energy neutron has been examined. Using the multiplicity results of MacDonald *et al.*,[32] it was found that fewer than one event in 400 was due to two or more lower-energy neutrons.

E. Conclusions on Neutron Spectra

The neutron energy spectra for the three elements studied are strikingly similar, although the

TABLE VII. Neutron energy spectra.

Target element	Minimum energy (MeV)	Maximum energy (MeV)	Neutrons per capture per MeV	Error	Integral spectrum	
					Neutrons per capture	Error
Run II Silicon	7.73	11.49	0.0251	0.0044	0.232	0.041
	11.49	15.62	0.0138	0.0024	0.138	0.025
	15.62	19.54	0.0087	0.0015	0.081	0.015
	19.54	24.55	0.004 61	0.000 82	0.0469	0.0086
	24.55	29.41	0.002 10	0.000 39	0.0238	0.0045
	29.41	35.34	0.001 32	0.000 25	0.0136	0.0026
	35.34	52.53	0.000 336	0.000 065	0.0058	0.0011
Run III Silicon	4.25	7.73	0.0522	0.0094	0.429	0.077
	7.73	11.49	0.0288	0.0050	0.247	0.044
	11.49	15.62	0.0157	0.0028	0.139	0.025
	15.62	19.54	0.0091	0.0016	0.074	0.014
	19.54	24.55	0.004 07	0.000 74	0.0382	0.0072
	24.55	29.41	0.001 71	0.000 33	0.0178	0.0035
	29.41	35.34	0.001 15	0.000 23	0.0095	0.0019
	35.34	52.53	0.000 158	0.000 033	0.002 71	0.000 57
Run II Sulfur	7.73	11.49	0.0234	0.0041	0.210	0.037
	11.49	15.62	0.0132	0.0023	0.122	0.022
	15.62	19.54	0.0070	0.0012	0.068	0.013
	19.54	24.55	0.004 01	0.000 72	0.0403	0.0077
	24.55	29.41	0.001 91	0.000 37	0.0202	0.0041
	29.41	35.34	0.001 14	0.000 23	0.0109	0.0023
	35.34	52.53	0.000 243	0.000 056	0.004 18	0.000 96
Run II Calcium	7.73	11.49	0.0210	0.0036	0.183	0.032
	11.49	15.62	0.0111	0.0019	0.104	0.019
	15.62	19.54	0.0062	0.0011	0.058	0.011
	19.54	24.55	0.003 30	0.000 59	0.0335	0.0063
	24.55	29.41	0.001 52	0.000 29	0.0170	0.0034
	29.41	35.34	0.000 94	0.000 19	0.0096	0.0020
	35.34	52.53	0.000 233	0.000 049	0.004 01	0.000 84
Run III Calcium	4.25	7.73	0.0480	0.0086	0.346	0.061
	7.73	11.49	0.0205	0.0036	0.179	0.031
	11.49	15.62	0.0121	0.0021	0.102	0.018
	15.62	19.54	0.0058	0.0010	0.0518	0.0092
	19.54	24.55	0.002 82	0.000 50	0.0290	0.0052
	24.55	29.41	0.001 54	0.000 28	0.0149	0.0027
	29.41	35.34	0.000 79	0.000 15	0.0074	0.0014
	35.34	52.53	0.000 156	0.000 029	0.002 68	0.000 49

number of neutrons per MeV per capture decreases slightly with increasing atomic number.

Several other experiments have been performed in which the energy spectrum of neutrons emitted following muon capture has been measured.

Hagge[33] measured the spectrum for calcium and other targets by using a liquid scintillation counter and unfolding the pulse-height spectrum. The energy interval from 2 to 16 MeV was covered, but the spectrum was not normalized to the number of muon captures. However, the slope of the spectrum can be compared to the slope of our spectrum in the energy region common to the two experiments. Our run III calcium data yielded a ratio of 0.428 for the ratio of the second bin to the lowest-energy bin, with an error between 0.107 and 0.165, depending on the degree of dependence of the errors. Hagge's spectrum yielded a ratio of 0.533 with an error of 0.032 to 0.090 for the corresponding energy region. The ratio of our third to second bin yielded 0.59 ± 0.15 to 0.22, and Hagge's spectrum yielded 0.66 ± 0.09 to 0.23 for the same energy region. The two experiments are seen to be in good agreement to the extent to which they can be compared.

Turner[34] measured the spectrum of muon-capture neutrons, using calcium and lead targets, in the energy interval 4 to 50 MeV. The neutron energy was determined from the range and direction of a proton recoil in a hydrogen bubble chamber. Turner's spectrum was normalized, and yielded an integral of 0.187 ± 0.047 neutrons with energy above 7.73 MeV per muon capture. Integrating over the same energy region, our run II yielded 0.183 ± 0.032 neutrons per muon capture, and run III yielded 0.179 ± 0.031 neutrons per muon capture. The shapes of our spectra are also in good agreement with Turner's.

Krieger[35] has measured the spectrum of neutrons emitted following muon capture in calcium. His integral spectrum is in agreement with ours, but his spectrum falls off less rapidly with increasing energy than does ours. Evseev *et al.*[36] have measured the neutron energy spectrum at low energies, and observe fine structure in the spectrum, which is attributed to giant resonances.

The neutron energy spectrum can be regarded as the sum of three contributions: evaporation neutrons, giant resonance neutrons, and direct neutrons. Since the first two contributions involve the formation of an intermediate nuclear state, only the direct neutrons can exhibit an asymmetry, unless the giant-resonance widths are sufficient that opposite-parity states overlap.

Turner[34] obtains 0.5 MeV for the nuclear temperature of calcium in muon capture. This result and the total number of neutrons per muon capture[32] indicate that the contribution of evaporation neutrons to the portion of the spectrum observed in this experiment is negligible.

The contribution of the giant-resonance spectra has been computed in the case of calcium by Überall.[37] Giant dipole resonances are expected to produce peaks in the neutron energy spectrum at 5.8, 10.3, 10.8, and 11.3 MeV. A calculation of the giant resonance levels has been performed by Foldy and Klein[38] for the cases of muon capture by ^{16}O and ^{40}Ca. They find a residual excitation energy of about 12 MeV in ^{40}K following muon capture by ^{40}Ca. Since the binding energy of the highest neutron level in ^{40}K is 8 MeV, their calculation indicates that the highest energy that a neutron emitted following capture to one of the principal giant-resonance states can have is 4 MeV. Such a neutron would not be observed in the present experiment.

Calculations of the directly emitted neutron energy spectrum have been performed by a number of authors. A calculation by Lubkin,[4] using a modified Fermi-gas model, predicts a high-energy limit of 11 MeV for capture by ^{40}Ca, and a rate more than 10 times smaller than that observed in this experiment. Shell-model calculations[39] predict a spectral shape which agrees well with this experiment, but predict a rate which is smaller by at least a factor of 8 than that observed in the present experiment. A more recent shell-model calculation by Bogan,[7] which uses an effective nucleon mass of 0.6, predicts a direct-energy spectrum which is in excellent agreement with the energy spectra observed in this experiment in the region above 25 MeV. See Fig. 17. Bogan's spectrum is smaller than the observed spectrum below 25 MeV, as one would expect if there are giant-resonance and evaporation contributions in this region. Similar results were obtained by Piketty and Procureur.[8] As mentioned in Sec. III they have shown that, whereas final-state interactions play a role in setting the level of normalization of the spectra, as expected, spin orbit terms do not. Examples from these papers are shown in Fig. 17 together with spectra observed in this experiment.

ACKNOWLEDGMENTS

The collaboration of A. Suzuki and K. Takahashi during the earlier phases of this experiment is most gratefully acknowledged. The authors also wish to thank Dr. P. D. Gupta for his assistance during run III, and to thank the staff of the Nuclear Research Center for their work on this experiment, most particularly our technicians J. Smith and F. Johns.

APPENDIX A. MUON-γ-NEUTRON TIME OF FLIGHT

In run I, the reaction sought was the capture of a muon by a target nucleus, followed by the emission of a neutron and the formation of an excited state in the daughter nucleus. In most cases, the lifetimes of the excited states of the daughter nuclei are sufficiently short compared to the neutron time of flight that they can be neglected. In this case the γ ray carries information of the time of capture of the muon. Counter 5 was used to detect the γ rays, with its pulse-shape discriminator output and with counters 6 and 9 in anticoincidence. Counter 7, located 1 m from the target, was used with counter 8, located directly in front of it, in anticoincidence, to detect neutrons and γ rays from the target. As in runs II and III, a precession magnet was used to precess the direction of the muon's spin.

The time between a muon stop and a γ event in counter 5 was measured by a digital timing system. The time between the γ event in counter 5 and a neutron or γ event in counter 7 was measured by a time-to-pulse-height converter. A two-dimensional analyzer was used to store the outputs from the digital timing system and from the time-to-pulse-height converter.

Since the angular distribution of the γ rays with respect to the direction of the muon spin is isotropic, the angular distribution of the neutrons with respect to the direction of the muon spin determines the amplitude modulation of the exponential decay curve, due to the precession of the direction of the muon spin. The energy of the neutron was determined from its time of flight. The advantage of measuring the asymmetry by this technique was that the neutron energy was determined directly by its time of flight, and no unfolding process was involved.

No values for the neutron asymmetry were obtained from run I because the even rate was much smaller than had been anticipated in planning the experiment. It has been assumed that the emission of a neutron did not strongly reduce the probability that a γ ray would be emitted. However, separate measurements of the numbers of neutrons emitted and the numbers of γ rays emitted indicated that the emission of a neutron with energy above 5 MeV reduced the probability of the emission of a γ ray by approximately a factor of 10.

Another problem associated with this method was the occurrence of half-real events. A muon stop followed by an accidental neutron and an accidental γ ray would produce a flat digital timing background which could be unambiguously subtracted. However, if either the γ or neutron, but not both, was real, the associated digital timing spectrum would have the same shape as a completely real-event spectrum. This required the use of delayed events to determine the background accurately.

The small real-event rates combined with the problems associated with half-real events made it impractical to measure the neutron asymmetry using the muon-γ-neutron time-of-flight technique

APPENDIX B. NEUTRON-γ COUNTER

Counter 5 was used to separate neutrons from γ rays by pulse-shape discrimination.

The scintillant consisted of a 19-cm-diam by 12.7-cm-long volume of NE-213 liquid scintillator, enclosed in a glass cell viewed by a 58AVP photomultiplier through a 0.61-m-long acrylic light pipe to permit thorough magnetic shielding of the photomultiplier.

The time distribution of the light output of the scintillant can be approximated as the sum of two exponentials, one having a time constant of 2.4 nsec, and the other having a time constant of 300 nsec.[40] These two components were integrated separately, multiplied by appropriate scale factors, and subtracted. The ratio of the slow component to the fast component is dependent upon the charge and velocity of the particle producing the light. Heavy particles from neutron interactions produce a higher ratio of slow to fast components than do electrons from γ-ray interactions.

The linearity of the counter was checked and found to be satisfactory using the half-fall points of the Compton edges of γ rays from ^{137}Cs, ^{60}Co, ^{24}Na, and ^{12}C*. The radial uniformity of counter 5 was checked using a highly collimated γ-ray beam. The root-mean-square fractional deviation of the pulse height from the average was 0.012. The number of photoelectrons per electron equivalent MeV was determined using a light pulser, and was found to be 165 photoelectrons per MeV. This number was used in the Monte Carlo computations.

Since the pulse height in counter 5 was used to determine the energy of neutrons, it was necessary to determine the relationship between the energy of a recoil proton and the pulse height that it produced. This was done by placing counter 5 a distance of 1.5 m from the target, stopping negative pions in the target, and selecting approximately monoenergetic neutrons by time of flight. The pulse-height spectrum was measured for a number of different neutron energies, and the upper edges of these spectra yielded the pulse height produced by a proton having nearly the same energy as the incident neutron. These results, shown in Fig. 18, were fitted to the integral of Birks's expression for specific light output,[41] $-dx(dE/dx)/E_0(1+kBdE/d.$, where E_0 is the initial proton energy and k and B are constants. The value of kB was obtained by a least-squares fit, and the fitted curve is shown in Fig. 18. The value obtained for kB was found to be 0.010 15 g/MeV cm^2.

The pion-capture time-of-flight measurement was also used to check the performance of the pulse-shape discriminator. Time-of-flight spectra were taken both ungated and gated by the pulse-shape discriminator. The absence of particles traveling at the speed of light in the group identified as neutrons, without reduction of the number of lower-velocity particles, indicated that the pulse-shape discriminator was operating properly.

In run II, the pulse-shape discriminator was set for optimum separation of γ rays and neutrons. The performance of the pulse-shape discriminator was continually monitored by means of a scatter plot of pulse height vs pulse-shape amplitude displayed on an oscilloscope. The pulse shape was also pulse height analyzed as a function of counter 5 pulse height, with and without gating by the pulse-shape discriminator. It was found that in the worst case approximately 0.4% of the γ rays were identified as neutrons, and 5.0% of the neutrons were identified as γ rays. In run III the latter spectra were taken both with counters 6 and 9 in coincidence and in anticoincidence. They were also taken gated by the pulse-shape discriminator and ungated. The spectra taken in coincidence with counters 6 and 9 consisted of electrons only, whereas the spectra taken in anticoincidence with 6 and 9 consisted of γ rays and neutrons. By a comparison of the part of the γ-plus-neutron spectrum which had the same shape as the electron spectrum to obtain an amplitude normalization, it was possible to determine the shape of the spectrum associated with neutrons only. These spectra permitted the fraction of γ rays and neutrons misidentified to be unambiguously determined.

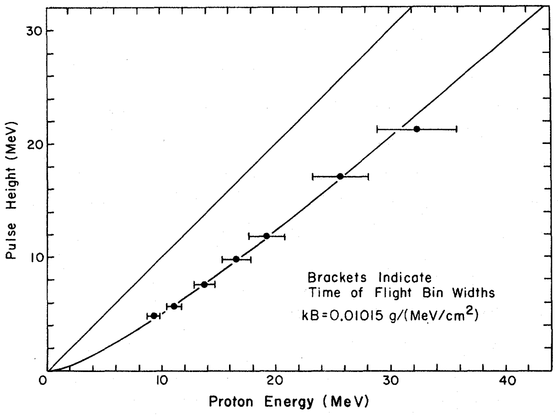

FIG. 18. Pulse-height response of NE-213 scintillator to protons.

In run III, the asymmetry data and the spectrum data were taken separately. For the asymmetry measurements, the pulse-shape discriminator was set so that practically no γ rays were identified as neutrons, and a correspondingly larger fraction of neutrons were identified as γ rays. The identification of neutrons as γ rays reduced the number of events recorded, but had no effect on the asymmetry value measured. For the neutron-spectrum measurements, the pulse-shape discriminator was set for optimum separation of γ rays and neutrons, and a small correction was made for the number of each misidentified as the other.

---

†Work supported in part by the U. S. Atomic Energy Commission.

*Present address: Laboratory of Nuclear Studies, Cornell University, Ithaca, New York 14850.

[1] C. S. Wu, E. Ambler, R. W. Hayward, D. D. Hoppes, and R. P. Hudson, Phys. Rev. 105, 1413 (1957); R. L. Garwin, L. M. Lederman, and M. Weinrich, *ibid.* 105, 1415 (1957); J. I. Friedman and V. L. Telegdi, *ibid.* 105, 1681 (1957).

[2] H. Primakoff, Rev. Mod. Phys. 31, 802 (1959).

[3] A striking example to the contrary is provided by muon capture in liquid hydrogen. See Ref. 2.

[4] E. Lubkin, Ann. Phys. (N.Y.) 11, 414 (1960).

[5] J. Rosen, private communication.

[6] R. Klein, R. Neal and L. Wolfenstein, Phys. Rev. 138, B86 (1965).

[7] A. Bogan, Jr., Phys. Rev. Letters 22, 71 (1969); Nucl. Phys. 12B, 89 (1969).

[8] C. A. Piketty and J. Procureur, Nucl. Phys. B26, 390 (1971).

[9] M. L. Yovnovich and V. S. Evseev, Phys. Letters 6, 333 (1963).

[10] R. M. Sundelin, R. M. Edelstein, A. Suzuki, and K. Takahashi, Phys. Rev. Letters 20, 1198 (1968).

[11] R. M. Sundelin, R. M. Edelstein, A. Suzuki, and K. Takahashi, Phys. Rev. Letters 20, 1201 (1968).

[12] R. M. Sundelin and R. M. Edelstein, in *Proceedings of the Third International Conference on High-Energy Physics and Nuclear Structure, 1969*, edited by S. Devons (Plenum, New York, 1970), p. 150; R. M. Sundelin, R. M. Edelstein, and P. D. Gupta, Bull. Am. Phys. Soc. 14, 50 (1969).

[13] R. M. Sundelin, Rev. Sci. Instr. 39, 251 (1968).

[14] R. M. Sundelin and K. Takahashi, Nucl. Instr. Methods 54, 250 (1967).

[15] M. Bardon, D. Berley, and L. M. Lederman, Phys. Rev. Letters 2, 56 (1959).

[16] M. Eckhause, R. T. Siegel, and R. E. Welsh, Nucl. Phys. 81, 575 (1966).

[17] J. Sculli, Columbia University Report No. NEVIS-168,

1969 (unpublished).

[18] See Refs. 19–26.

[19] C. T. Coffin, A. M. Sachs, and D. H. Tycko, Bull. Am. Phys. Soc. 3, 52 (1958).

[20] W. F. Baker and C. Rubbia, Phys. Rev. Letters 3, 179 (1959).

[21] V. S. Evseev, V. I. Komarov, V. Kush, V. S. Roganov, V. A. Chernogorova, and M. Szymczak, Acta Phys. Polonica 21, 313 (1962); V. S. Evseev, V. S. Roganov, V. A. Chernogorova, Chang Run-Hwa, and M. Szymczak, Phys. Letters 6, 332 (1963); V. S. Evseev, V. S. Roganov, V. A. Chernogorova, Chang Run-Hwa, and M. Szymczak, Yadern. Fiz. 4, 342 (1966) [transl.: Soviet J. Nucl. Phys. 4, 245 (1967)]; V. S. Evseev, F. Kilbinger, V. S. Roganov, V. A. Chernogorova, and M. Szymczak, Yadern. Fiz. 4, 545 (1966) [transl.: Soviet J. Nucl. Phys. 4, 387 (1967)]; see also Refs. 22 and 24.

[22] V. S. Evseev, V. I. Komarov, V. Z. Kush, V. S. Roganov, V. A. Chernogorova and M. Szymczak, J. Exptl. Theoret. Phys. 41, 306 (1961).

[23] E. W. Anderson and J. E. Rothberg, Bull. Am. Phys. Soc. 10, 80 (1965); E. W. Anderson, Columbia University Report No. NEVIS-136, 1965 (unpublished).

[24] V. S. Evseev, V. S. Roganov, V. A. Chernogorova, M. M. Szymczak, and Chang Run-Hwa, in *Proceedings of the Conference on High-Energy Physics at CERN* (CERN, Geneva, 1962), p. 425.

[25] A. Astbury, I. M. Blair, M. Hussain, M. A. R. Kemp, H. Muirhead, and R. G. P. Voss, Phys. Rev. Letters 3, 476 (1959); A. Astbury, J. H. Bartley, I. M. Blair, M. A. R. Kemp, H. Muirhead, and T. Woodhead, Proc. Phys. Soc. (London) 79, 1011 (1962).

[26] V. L. Telegdi, in *Proceedings of the Rochester Conference on High-Energy Physics, 1960* (Univ. of Rochester, Rochester, N.Y., 1960), p. 713.

[27] M. Rho, in *Proceedings of the Third International Conference on High-Energy Physics and Nuclear Structure, 1969,* edited by S. Devons (Plenum, New York, 1970), p. 122; A. Fujii, R. Leonardi, and M. Rosa-Clot, *ibid.*, p. 171; V. V. Balashov, R. A. Eramzhyan, N. M. Kabchnik, G. Ya. Korenman, and V. L. Korotkin, *ibid.*, p. 174.

[28] *Neutron Cross Sections,* compiled by D. Hughes and R. Schwartz, Brookhaven National Laboratory Report No. BNL-325 (U. S. GPO, Washington, D. C., 1958).

[29] M. Goldberg, V. May, and J. Stern, Brookhaven National Laboratory Report No. BNL-400, 1962 (unpublished).

[30] J. B. Birks, Proc. Phys. Soc. (London) 64A, 874 (1951).

[31] R. Huff, University of Chicago Report No. EFINS-61-27, 1961 (unpublished).

[32] B. MacDonald, J. Diaz, S. Kaplan, and R. Pyle, Phys. Rev. 139, B1253 (1965).

[33] D. Hagge, University of California Report No. UCRL-10516, 1963 (unpublished).

[34] L. Turner, Carnegie Institute of Technology Report No. CAR-882-5, 1964 (unpublished).

[35] M. H. Krieger, Columbia University Report No. NEVIS-172, 1969 (unpublished).

[36] V. S. Evseev, T. Kozlowski, V. Roganov, and J. Woitkowska, Phys. Letters 28B, 553 (1969); V. S. Evseev, T. Kozlowski, V. Roganov, and J. Woitkowska, in *Proceedings of the Third International Conference on High-Energy Physics and Nuclear Structure, 1969,* edited by S. Devons (Plenum, New York, 1970), p. 157.

[37] H. Überall, Phys. Rev. 139, B1239 (1965).

[38] L. L. Foldy and R. H. Klein, Case Institue of Technology and Western Reserve University Report No. COO-1573-14, 1967 (unpublished).

[39] E. Dolinskii and L. Blokhintsev, J. Exptl. Theoret. Phys. 35, 1488 (1958); M. Akimova, L. Blokhintsev, and E. Dolinskii, *ibid.* 39, 1806 (1960).

[40] R. B. Owen, IEEE Trans. Nucl. Sci. NS5, 198 (1958).

[41] E. J. Bowen, E. Mikiewicz, and F. W. Smith, Proc. Phys. Soc. (London) 62A, 26 (1949); also see Ref. 30.